JOC The Journal of Organic Chemistry

Article

pubs.acs.org/joc

Conformational Control in [22]- and [24]Pentaphyrins(1.1.1.1.1) by Meso Substituents and their N-Fusion Reaction

Mercedes Alonso,* Paul Geerlings, and Frank De Proft

Eenheid Algemene Chemie (ALGC), Vrije Universiteit Brussel (VUB), Pleinlaan 2, 1050 Brussels, Belgium

Supporting Information

ABSTRACT: *meso*-Substituted pentaphyrins(1.1.1.1.1) were unexpectedly isolated as N-fused species under Rothemund-type conditions. The reaction mechanism is unknown at present, but the first example of a nonfused [22]pentaphyrin was reported in 2012. Here, the conformational preferences and N-fusion reaction of [22]- and [24]pentaphyrins have been investigated using density functional calculations, together with their aromaticity-molecular topology relationships. Two global minima are found for the unsubstituted [22]pentaphyrin corresponding to *T0* and $T0^{4,D}$ Hückel structures. Möbius transition states are located in the interconversion pathways with activation barriers of 27 kcal mol^{-1}. Conversely, [24]pentaphyrin is able to switch between Hückel and Möbius conformers with very low activation barriers. However, nonfused [24]pentaphyrins are unstable and spontaneously undergo an N-fusion reaction driven by the strain release. On the contrary, nonfused [22]pentaphyrins could be isolated if a $T0^{4,D}$ conformation is adopted. Importantly, conformational control of pentaphyrins can be achieved by *meso*-substituents. Two stable conformations ($T0^{4,D}$ and $T0^{A,D}$) are found for the nonfused [22]pentaphyrin, which are delicately balanced by the number of substituents. The $T0^{A,D}$ conformation is preferred by fully *meso*-aryl pentaphyrins, which is converted to the N-fused species. Interestingly, the removal of one aryl group prevents the N-fusion reaction, providing stable aromatic nonfused [22]pentaphyrins in excellent agreement with the experimental results.

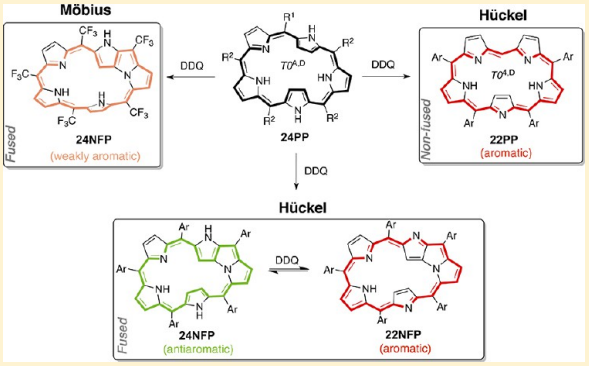

INTRODUCTION

The fascinating concept of Möbius aromaticity, which predicts that [4*n*]annulenes with a twisted Möbius-strip topology are aromatic, was proposed by Heilbronner in 1964.[1] However, the first stable Möbius molecule was characterized only in 2003,[2] although its aromatic character was argued with respect to the large dihedral angle and magnetic aromaticity criteria.[3] In [4*n*]annulenes, the small *cis-trans* isomerization barriers makes the "locking in" of a twisted Möbius structure very difficult.[4] Interestingly, expanded porphyrins with more than four pyrrole rings overcome this problem, taking advantage of their conformational flexibility and multiple oxidation states.[5,6] The first example was a di-*p*-benzi[28]hexaphyrin reported by Latos-Grażiński and co-workers that exhibits a Möbius structure in the solid state but shows a temperature-dependent conformational change between Hückel antiaromatic and Möbius aromatic species in solution.[7]

Extensive studies by Osuka et al. led to the discovery of expanded porphyrins with distinct aromaticity and singly twisted topology,[5a] including [28]hexaphyrin,[8] [32]heptaphyrin,[9] and [36]octaphyrin[10] containing single-carbon meso bridges. Metalation,[11] protonation,[12] or intramolecular fusion reactions[13] are different methods to achieve Möbius aromatic molecules from expanded porphyrins. Besides the Möbius topology, these macrocycles adopt a variety of intriguing structures,[6a] such as planar or chiral figure-eight conformations, which can be interconverted under certain conditions. To date, several expanded porphyrins have been reported that switch between two, and even three, distinct π-conjugation topologies, with different absorption and emission spectra.[14] Such a change of topology involves a Hückel−Möbius aromaticity switch,[15] and it can be induced by solvent, temperature, and pH, among others.[16]

Interestingly, the photophysical properties are strongly dependent on the aromatic versus antiaromatic character of the π-electron system.[17] Hückel and Möbius aromatic expanded porphyrins exhibit distinct absorption spectra with B- and Q-like bands, strong fluorescence, long-lived excited states, and large two-photon absorption (TPA) cross-sections.[14] Therefore, these large π-conjugated macrocycles are promising candidates for two-photon absorption[18] and near-infrared dyes.[19]

Among porphyrinoids, pentapyrrolic macrocycles have attracted attention as potential drug leads for photodynamic therapy.[20] Five different pentaphyrin structures containing only one-carbon *meso* bridges have been already synthesized,[5b] and the largest TPA cross-section value corresponds to the β-substituted pentaphyrin(1.1.1.1.1) with five methine bridges.[21] This compound was proven to be aromatic in line with the 22π-electron configuration predicted by the annulene model.[22] However, attempts to synthetize fully *meso*-substituted penta-

Received: February 26, 2013
Published: April 3, 2013

phyrins(1.1.1.1.1) resulted unexpectedly in the isolation of N-fused systems in two stable oxidation states, corresponding to 22π- and 24π-electrons ([22]NFP and [24]NFP).[23] Importantly, [24]NFP provided the smallest Möbius aromatic system with a distinct diatropic current upon Rh(I) metalation.[24] The mechanism for this unique N-fusion reaction is not clarified yet, although only β-alkylated regular pentaphyrins were isolated as stable nonfused macrocycles.[25] Remarkably, larger *meso*-aryl substituted expanded porphyrins, such as hexaphyrins(1.1.1.1.1.1), provided stable nonfused structures under similar Rothemund-type conditions.[26] Only, very recently, the first example of a β-unsubstituted nonfused [22]-pentaphyrin(1.1.1.1.1) with a free *meso* position was reported.[27]

Although there are extensive studies on pentapyrrolic macrocycles like sapphyrins, little attention has been given to regular pentaphyrins(1.1.1.1.1). Herein, a thorough quantum chemical study is carried out focusing on diverse properties of [22]- and [24]pentaphyrins(1.1.1.1.1) ([22]PP and [24]PP), including conformational analysis, topology switching and their N-fusion reaction. It is shown that conformational control of these pentapyrrolic macrocycles can be achieved by *meso*-substituents. Importantly, the chemical stability of nonfused pentaphyrins is critically dependent on the number of aryl groups at the *meso* positions. A large conformational change in [22]PP is caused by the removal of one *meso*-substituent, preventing the spontaneous N-fusion reaction in *meso*-free pentaphyrins.

The aim of this work is 2-fold. First, the viability of Möbius topologies in [22]- and [24]pentaphyrins(1.1.1.1.1) (**1**-**4**, Scheme 1) is analyzed using density functional theory

Scheme 1. Hückel Conformations of [22]- and [24]Pentaphyrins and Their N-Fused Products

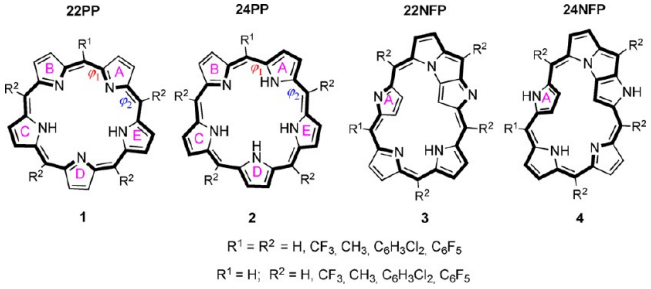

calculations. Previously, we have shown that aromatic Möbius structures are easily achieved in [28]hexaphyrin[28] and protonated [32]heptaphyrin[29] but not for [26]hexaphyrin, which strongly preferred aromatic planar conformations. On the other hand, porphyrins proved to be too small to allow Möbius topologies due to excessive ring strain.[28] Second, we describe the structure−property relationships between molecular topology, aromaticity, and band gaps in pentaphyrins. Aromaticity has been quantified using several energetic, structural, magnetic, and reactivity criteria. Since most of the indices have been developed for the particular case of planar aromatic systems, it is important to assess the performance of the different indices to describe Möbius aromaticity.

COMPUTATIONAL METHODS

All calculations have been performed with the Gaussian 09 program[30] using the three-parameter B3LYP functional[31] with the 6-31G(d,p) basis set. In previous works, B3LYP was concluded to show the best overall performance for describing geometries and thermochemistry of hexaphyrins and heptaphyrins.[28] Modern functionals such as M06-2X were proved to underestimate the degree of bond-length alternation and failed to correctly predict the stability of the Möbius conformer in protonated [32]heptaphyrin.[29] The use of a larger basis set like 6-311+G(d,p) resulted in very small changes in the relative energies and activation barriers.[28] In any case, the performance of the empirical dispersion correction (DFT-D) on the geometries and energies of several pentaphyrins has been also assessed.[32]

The geometries of Hückel and Möbius conformers of pentaphyrins **1** and **2** were fully optimized and characterized by harmonic vibrational frequency computations. The zero-point vibrational energy (ZPE) and the thermodynamic contributions to the enthalpies (ΔH) and Gibbs free energies (ΔG) were computed at 298 K and 1 atm. The topological descriptor Tn^X indicates the number of half-twists (n) and the subunits located between two transoid linkages (X).[5b]

Relaxed potential energy (PES) surfaces for **1** and **2** were performed at the B3LYP/6-31G(d,p) level in order to locate the most stable conformations and transition states. Two internal dihedral angles, centered on carbon−carbon bonds (φ_1 or φ_2 in Scheme 1), were chosen for constructing the 3D PES. All local minima and transition states were further optimized without any geometrical restriction and verified by frequency calculations. For the transition states, only one imaginary frequency was found corresponding to the rotation of these dihedral angles.

The isomerization method[33] was applied to evaluate the isomerization stabilization energies (ISEs), magnetic susceptibility exaltation[34] (Λ), and relative hardness[35] ($\Delta\eta$) of pentaphyrins **1** and **2**. The reactions that were used to compute the aromaticity indices of the Hückel [22]PP and the Möbius [24]PP are shown in Scheme 2. The *syn*-

Scheme 2. Reactions Used To Evaluate the Isomerization Stabilization Energy (ISE), the Magnetic Susceptibility Exaltation (Λ), and the Relative Hardness ($\Delta\eta$) of [22]PP and [24]PP[a]

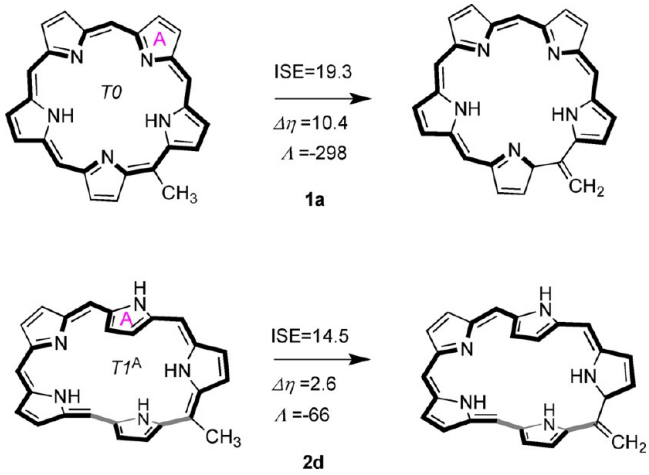

[a]ISE and $\Delta\eta$ are given in kcal mol^{-1} and Λ in ppm cgs.

anti corrections for the isomerization stabilization energies were evaluated as the energy difference between the dihydrogen derivative of the *meso*-methyl pentaphyrin and its respective nonaromatic isomer (Supporting Information). Systems with positive ISE values are aromatic, whereas those with strongly negative ISE values are considered to be antiaromatic. The magnetic susceptibilities were computed using the CSGT method[36] at the HF/6-31+G** level of theory, and the GIAO/B3LYP/6-311+G(d,p) method was used for the NICS (nucleus-independent chemical shifts) calculations.[37] NICS values were calculated at the geometrical center of the 30 heavy atoms of the pentaphyrin framework [NICS(0)] and at 1 Å above the ring center [NICS(1)]. Exaltations and NICS are negative (diamagnetic) for aromatic compounds and positive (paramagnetic) for antiaromatic systems.

dx.doi.org/10.1021/jo4003823 | J. Org. Chem. 2013, 78, 4419−4431

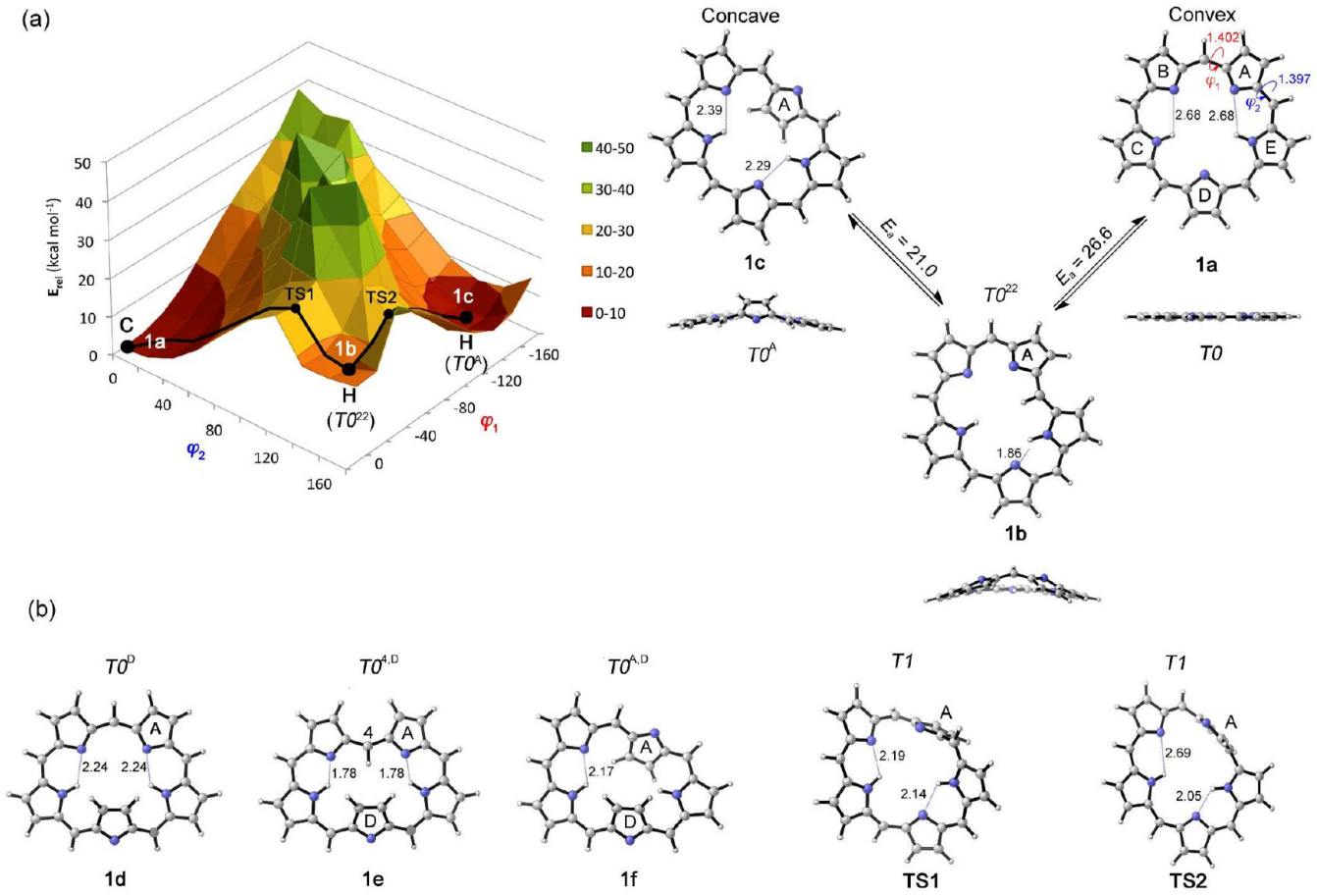

Figure 1. (a) B3LYP/6-31G(d,p) relaxed energy potential surface for the [22]pentaphyrin **1a** obtained by rotating the dihedral angles φ_1 and φ_2. (b) The fully optimized geometries for minima and transition states, with their corresponding hydrogen-bond distances (Å), are also shown. The conformational descriptor Tn^x is also displayed. *T0* and *T1* structures have Hückel and Möbius topology, respectively.

The relative hardness ($\Delta\eta$) is a reactivity descriptor of the aromaticity. In the past, large band gaps were associated with stable structures. This finding is nicely captured in the maximum hardness principle, which states that molecules will arrange themselves to be as hard as possible.[38] Using the maximum hardness principle, the methyl derivative is expected to be systematically harder than the methylene isomer in the aromatic compounds ($\Delta\eta > 0$) and vice versa in the antiaromatic systems ($\Delta\eta < 0$). The LUMO and HOMO energies were used for computing the hardness η of the methyl and methylene isomers involved in the isomerization method.

Ring strain was quantified using two torsional parameters: the average absolute deviation from either 0° and 180° of the dihedral angles along the classical conjugation pathway (ψ) and the average dihedral angle between the neighboring pyrrole rings (Φ_p). Since ψ and Φ_p are linearly correlated (Figure S2, Supporting Information), we only use Φ_p as a reference descriptor for the ring strain here. Since the evaluation of the ring strain is only based in the dihedral angles, Φ_p should be regarded as a "torsional strain" descriptor. Other contributions to the ring strain, such as bond angle distortions, are neglected by Φ_p. On the other hand, the extent of effective overlap of neighboring p orbitals was measured by the torsional π-conjugation index (Π),[5b] defined by Stępień as follows (eq 1)

$$\Pi = \prod_i \cos \varphi_i \qquad (1)$$

where φ_i are the dihedral angles along the conjugation pathway (CP). $\Pi = 1$ for a completely planar system, it is positive for any Hückel (double-sided) conformation and negative for any Möbius surface.

For the visualization of noncovalent interactions (NCI), we used the NCIPLOT program.[39] B3LYP/6-31G(d,p) wave functions and grids of 0.1 au were used.

RESULTS AND DISCUSSION

Unsubstituted [22] and [24] Nonfused Pentaphyrins. In order to identify the most stable conformations and the conversion pathways, we performed a series of 2D relaxed potential energy surface (PES) scans of **1**. Figure 1 shows the surface plot of the energy versus the dihedral angles φ_1 and φ_2 from the convex conformation **1a**, computed at the B3LYP/6-31G(d,p) level of theory. In the convex conformation, all subunits have a *cis-cis* alignment, so all nitrogen atoms point inward (Figure S1, Supporting Information).[5b] On the other hand, concave conformers contain inverted subunits (pyrrole rings and/or *meso*-bridges). Three minima with a Hückel topology were located (**1a**, **1b**, **1c**), and they were fully optimized at the same level. Additional minima were found on the potential energy surfaces of the concave conformers **1c** and **1d** (see Figure S3 in the Supporting Information). The 3D structures of the main conformations of the nonfused [22]PP are also shown in Figure 1.

In previous works, we proposed a set of simple descriptors to quantify independently ring strain, hydrogen bonding, and π-conjugation in Hückel and Möbius topologies.[28,29] The average dihedral angle between neighboring pyrrole rings (Φ_p) is used as a measure of torsional strain. The hydrogen-bonding index (N_H)

dx.doi.org/10.1021/jo4003823 | J. Org. Chem. 2013, 78, 4419−4431

Table 1. Relative Energies (E_{rel}), Topological Descriptor (Tn^X), Hydrogen Bonding (N_H), Torsional Strain (Φ_P), Maximum Deviation of Dihedral Angles from Planarity (ψ_{max}), π-Conjugation index (Π), and Bond Length Alternation (Δr_{C-N} and Δr_{C-C}) of Unsubstituted [22]PP and [24]PP Conformers[a,b]

conformer	Tn^X	E_{rel}	N_H	Φ_p	ψ_{max}	Π	Δr_{C-N}	Δr_{C-C}
				[22]pentaphyrin				
1a (H)	*T0*	0.00	2	0.0	0.0	1.00	0.002	0.069
1b (H)	$T0^{22}$	16.17	1	20.6	29.3	0.61	0.043	0.080
1c (H)	$T0^{A}$	4.86	2	17.0	28.9	0.50	0.060	0.105
1d (H)	$T0^{D}$	7.09	2	17.0	28.8	0.69	0.014	0.061
1e (H)	$T0^{4,D}$	0.09	2	21.8	24.8	0.71	0.012	0.065
1f (H)	$T0^{A,D}$	15.15	1	29.3	40.7	0.43	0.027	0.069
TS1 (M)	*T1*	26.6	2	44.1	61.5	−0.16	0.109	0.118
TS2 (M)	*T1*	25.81	2	37.5	79.6	−0.08	0.102	0.120
				[24]pentaphyrin				
2a (H)	*T0*	0.00	1.5	36.9	36.7	0.47	0.058	0.100
2b (M)	*T1*	2.80	1.5	44.8	70.1	−0.17	0.046	0.096
2c (H)	$T0^{A}$	5.39	1	27.5	47.4	0.50	0.060	0.105
2d (M)	$T1^{A}$	5.06	1	46.4	59.5	−0.17	0.029	0.083
2e (H)	$T0^{A,D}$	4.76	1	38.4	50.6	0.29	0.048	0.111
2d′ (M)	$T1^{A}$	9.58	1	49.9	66.8	−0.14	0.048	0.111
2e′ (H)	$T0^{A,D}$	4.69	1	43.4	38.8	0.34	0.059	0.104
2f (H)	$T0^{4,D}$	3.27	1	33.3	35.8	0.48	0.048	0.099

[a] E_{rel} are given in kcal mol^{-1}, Φ_p and ψ_{max} in deg, and Δr_{C-N} and Δr_{C-C} in Å. [b] H denotes a Hückel topology, whereas M corresponds to a Möbius topology.

indicates the number of intramolecular hydrogen bonds and assigns a value of 1 for single N−H···N bonds and 1.5 for bifurcated ones. On the other hand, the efficiency of π-conjugations is measured by the torsional π-conjugation index (Π). All of these descriptors together with the relative energies of the [22]PP conformers are collected in Table 1. The differences in length between the shortest and longest C−C and C−N bonds (Δr) are also included in Table 1, as a measure of bond length alternation.

The topology of a π-conjugated system is easily determined by examining torsional angles in the macrocycle. The system has a Möbius topology when the number of *trans* bonds in the smallest macrocyclic circuit (SMC) is odd.[5b,40] On the other hand, a Hückel conformer always contains an even number of *trans* bonds regardless of the inversion pattern. In the discussion, the different conformations are described using the topological descriptor Tn^x, which indicates the number of half-twists (n), namely linking number,[41] and the subunits (pyrrole rings and/or *meso* carbon atoms) located between two transoid linkages (X).

For unsubstituted nonfused [22]pentaphyrin, we found two degenerate global-energy minima: the convex conformation **1a** and a Hückel conformation with one inverted pyrrole **1e**. Whereas the convex structure **1a** is perfectly planar and ring-strain free, the two intramolecular hydrogen bonds are stronger in **1e** owing to the shorter NH···N distances and larger angles (Figure 1). Experimental studies showed that a convex conformation is preferred by β-alkylated [22]PP,[25] while 5,10,15,20-tetrakis(pentafluorophenyl) [22]PP adopts the conformation **1e**.[27]

As shown in Figure 1, the low energy pathway for the rotation of an imine-type pyrrole ring from the convex structure **1a** involves a two-step mechanism. The conversion of **1a** to **1c** involves one intermediate conformer **1b** upon rotation of the φ_2 torsion, which is 16 kcal mol^{-1} less stable than **1a**. A further rotation around φ_1 in **1b** led to the A-inverted conformer **1c**, only 4.9 kcal mol^{-1} higher in energy than the totally planar conformation **1a**. The overall activation barrier is fairly large (E_A = 26.6 kcal mol^{-1}), and distorted Möbius topologies were found as transition states. Delocalization in both **TS1** and **TS2** is inhibited by large dihedral angles (Table 1), which hinders effective π overlap. However, these singly twisted structures can be stabilized by hyperconjugation.[42] The bond-length alternation increases in the Möbius transition states (HOMA < 0.560), and slightly positive NICS values were obtained at the ring center. No local minima with nominal Möbius topology were found for [22]PP.

The inversion of the subunit D has a very similar potential energy surface compared to the $T0$−$T0^A$ conversion (Figure S3, Supporting Information), although the D-inverted conformer **1d** is 7.1 kcal mol^{-1} higher in energy than **1a** and the overall activation barrier is 26.8 kcal mol^{-1}. Interestingly, the relative stabilities of the conformations with an inverted pyrrole ring in [22]PP (**1c** and **1d**) are far below those in regular porphyrin, in which one inversion implies an increase in energy above 42 kcal mol^{-1}.[43] Thus, increasing the size of the macrocycle from porphyrins to pentaphyrins significantly provides more conformational flexibility. In fact, a conformation with two inverted pyrrole rings **1f**, named triangular, is also feasible in presence of some substituents (see below).

We considered the possibility of concerted ring inversion, but no transition states could be located for such pathways. In the case of imine-type pyrrole ring, stepwise mechanisms emerged. On the contrary, the inversion of the amine-type pyrrole ring C occurs via a one-step process involving a Möbius transition structure (Figure S3, Supporting Information). The activation barrier is 30.8 kcal mol^{-1} and the C-inverted conformer is 14.5 kcal mol^{-1} higher in energy than **1a**. The energetics of the pathways for the conformational changes in [22]PP are summarized in Figure 2. The red dotted line corresponds to the one-step mechanism found for the inversion of the amine-type pyrrole ring C.

Upon reduction, the macrocycle switches over to the [24] π-electron conjugation pathway, resulting in important changes on the conformational preferences. Even though the macrocycle is

dx.doi.org/10.1021/jo4003823 | J. Org. Chem. 2013, 78, 4419−4431

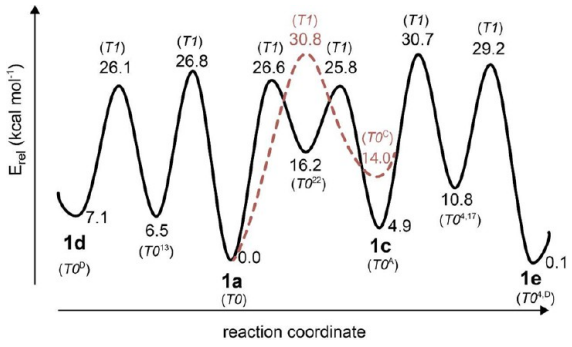

Figure 2. Energy diagram for the conformational interconversion pathways in [22]pentaphyrin. The dotted red line corresponds to the inversion of the amine-type pyrrole ring C.

antiaromatic according to Hückel's rule, unsubstituted [24]PP still prefers the convex conformation **2a** because of its more effective hydrogen bonding and lower torsional strain. However, the relative energies of most conformations are below 5 kcal mol^{-1}. The small energy differences in [24]PP can be rationalized in terms of planarity/aromaticity of the convex conformation. Unlike **1a** (Φ_p = 0), **2a** is highly distorted from planarity increasing enormously the torsional strain (Φ_p = 37). Furthermore, NICS computed at the center of the macrocycle **2a** has a large positive value of 22 ppm, corresponding to an antiaromatic structure. In contrast, **1a** is strongly aromatic (NICS = −15.6) and stabilized due to the [22]annulenoid system. Consequently, the thermodynamic stability of the convex conformation is significantly decreased in [24]PP.

The relaxed energy potential surface obtained by rotating the dihedral angles φ_1 and φ_2 from the convex conformation **2a** is displayed in Figure 3. The inversion of the pyrrole ring A in [24]PP involves a two-step mechanism with low activation energies. The rotation of φ_2 results in a Möbius-type conformation **2b** (with no imaginary frequencies), only 2.8 kcal mol^{-1} higher in energy than **2a**. This Hückel−Möbius topology switch requires a very low energy barrier (E_A = 2.84 kcal mol^{-1}). The *T1* structure **2b** is transformed into a Hückel *T0*^{A} conformer **2c** by rotating the adjacent φ_2. Compound **2c** is 5.4 kcal mol^{-1} less stable than **2a**, and the overall barrier for the **2a**→**2c** is 9.4 kcal mol^{-1}. In [24]PP, the energy barrier for *T0*→*T0*^{A} interconversion decreases by 17 kcal mol^{-1} compared to [22]PP. Previously, it was reported that the longer the rotating bond, the lower the rotational barrier.[44] Accordingly, the rotating bond in **2a** is 0.043 Å larger than that of **1a**.

Similar potential energy surfaces were obtained for the inversion of a second pyrrole ring in **2c**. Two quasi-degenerate *T0*^{A,D} isomers were located that differ in the relative orientation of the two inverted pyrrole rings (A and D). Whereas A and D face toward the same direction in **2e′**, they are stacked in **2e**. The triangular conformations lie only 5 kcal mol^{-1} higher in energy than **1a**. In both cases, a two-step mechanism via a Möbius *T1*^{A} intermediate corresponds to the lowest energy path for the *T0*^{A}→*T0*^{A,D} interconversion (Figure S4, Supporting Information). Figure 4 summarizes the B3LYP/6-31G(d,p) energetics for the different conformational interconversion pathways in [24]PP. For the stacked configuration, the Möbius and the Hückel conformations (**2d** and **2e**) are degenerate in energy, and its interconversion is practically a barrierless process. A *T0*^{4,D}

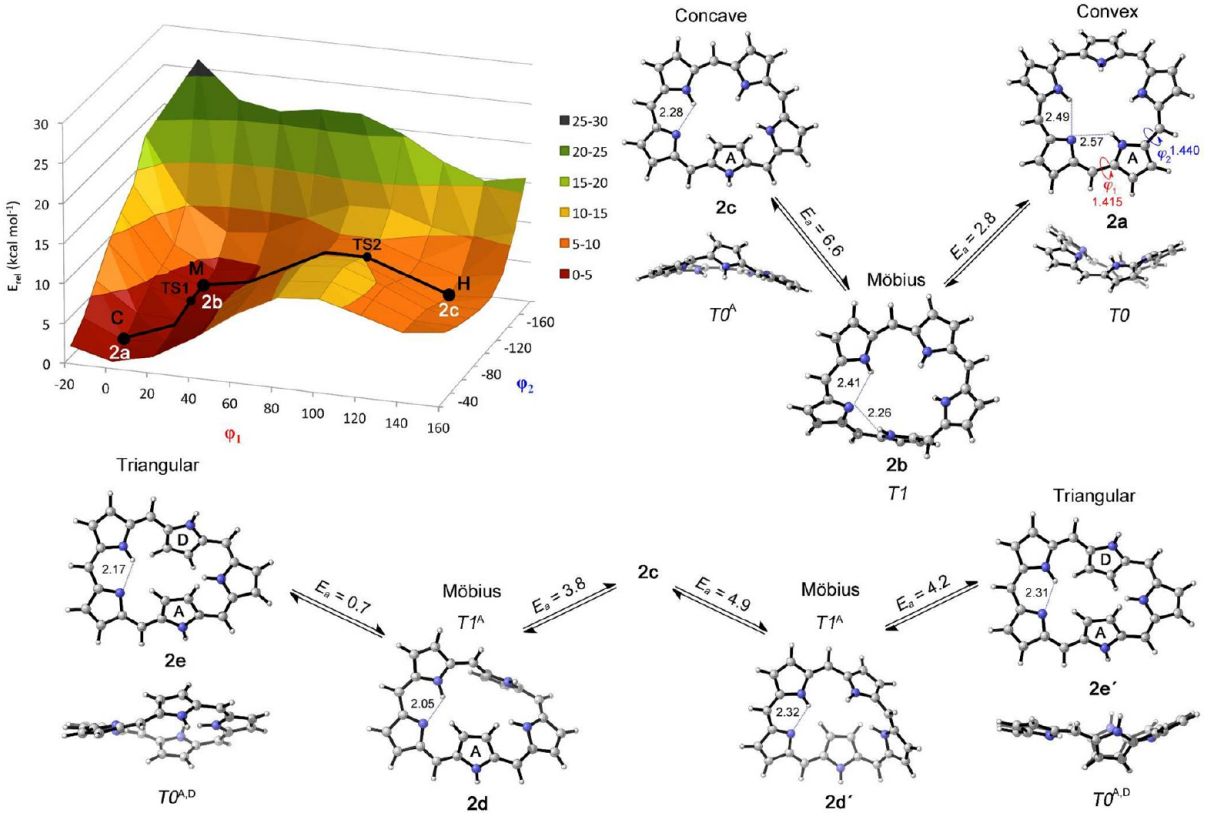

Figure 3. B3LYP/6-31G(d,p) relaxed energy potential surface for the [24]pentaphyrin **2a** obtained by rotating the dihedral angles φ_1 and φ_2. The fully optimized geometries for the minima together with the activation energy barriers and the hydrogen-bond and rotating-bond distances (Å) are shown. The conformational descriptor *Tn*^{x} is also displayed. All *T0* conformers have a Hückel topology.

dx.doi.org/10.1021/jo4003823 | J. Org. Chem. 2013, 78, 4419−4431

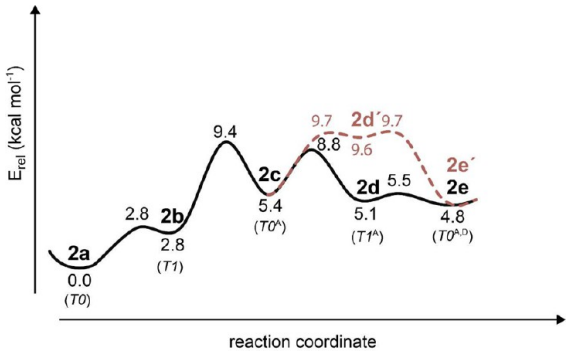

Figure 4. Energy diagram for the conformational interconversion pathways in [24]pentaphyrin.

structure **2f** is also possible for [24]PP. The relative energies together with the low activation energies suggest that all the conformations are readily accessible for [24]PP. As we will show later, the steric effects and the number of *meso* substituents control the conformational preference and stability of [22]- and [24]pentaphyrins. Solvent plays a minor role in the stability of the different conformers of nonfused pentaphyrins, as shown by the free solvation energies in THF and DMSO computed with the recently introduced solvation model SMD (Table S2, Supporting Information).[45]

It is important to stress that the inclusion of the DFT-D dispersion correction does not significantly affect the optimized geometries of **1a**−**f** and **2a**−**f** or the relative energies (Table S1, Supporting Information). The largest discrepancy between B3LYP and B3LYP-D corresponds to the stability of the $T0^{4,D}$ structures **1e** and **2f**. According to B3LYP-D, this conformation is lower in energy than the convex conformation **1a** in [22]PP and almost degenerate with **2a** in [24]PP. The mean absolute difference between B3LYP and B3LYP-D relative energies is small with a mean absolute difference of 2.0 kcal mol^{-1}.

Although the Möbius topology is indeed accessible for [24]PP, it does not exhibit a distinct macrocyclic aromaticity, as **2b** and **2d** have $\Pi = -0.17$. Normally, macrocyclic aromaticity is associated with expanded porphyrins having Π values higher than 0.3.[5b] The worst dihedral angles along the CP are 70.1 in **2b** and 59.5° in **2d**, respectively. It is worth noting that the aromatic Möbius topologies of the [28]hexaphyrin and [32]heptaphyrin are characterized by fairly smooth π-conjugation surfaces with $\Pi > -0.5$.[28,29]

Linear regression analysis shows that the conformational stabilities in the [22]PP are mainly governed by torsional strain (Figure S6, Supporting Information). However, hydrogen bonding seems to be the main factor governing the relative energies of the [24]PP conformers. It is interesting to note that the relative energy does not correlate with any of the aromaticity parameters. However, even though Möbius conformations of [22]- and [24]PP have similar ring strain according to Φ_p, the single-sided topologies are transition states highly destabilized in the [22]PP. Therefore, the aromatic stabilization effect should be important for these conformations being minima on the PES of [24]PP.

Aromaticity of Nonfused [22]- and [24]Pentaphyrins. The annulene model is widely used to predict the aromaticity of porphyrinoids.[46] According to this model, the ring system of a porphyrinoid is treated as a bridged heteroannulene, so aromaticity can be predicted by formally applying the [4*n*+2] Hückel rule to the annulene substructure.[47] However, these macrocycles sustain multiple conjugation pathways and, in principle, the Hückel rule should not be applied to polycyclic π-systems. Very recently, Aihara et al. have shown that the main macrocyclic conjugation pathway in regular and N-fused porphyrinoids predicted by graph-theoretical procedures is exactly the same as that predicted by the annulene model.[48] Macrocyclic aromaticity can be broadly predicted from the nominal number of π-electrons in the annulene-like CP,[49] although pyrrole rings seem to be a major source of the aromatic stabilization of the regular porphyrin.[50]

We have explored the aromaticity−molecular topology relationship in nonfused [24]- and [22]pentaphyrins based on several aromaticity criteria, so further insight into the validity of the annulene model can be provided. The degree of aromaticity in **1a**−**f** and **2a**−**f** has been quantified using the structural (HOMA),[51] magnetic (NICS, Λ),[34,37] energetic (ISE),[33] and reactivity ($\Delta\eta$)[35] aromaticity indices. Previously, we have proved that the isomerization method is very effective in evaluating aromatic stabilization energies (ISEs), magnetic susceptibility exaltation (Λ), and relative hardness ($\Delta\eta$) of Hückel and Möbius expanded porphyrins.[28,29] The aromaticity descriptors are collected in Table 2.

Table 2. Energetic, Reactivity, Magnetic, and Structural Indices of Aromaticity[a]

compd	top[b]	ISE	ISE_{corr}	$\Delta\eta$	Λ	NICS	$NICS_{zz}(1)$	HOMA
benzene	H	34.4	34.3	55.3	−18	−8.0	−29.2	0.982
				[22]pentaphyrins				
1a (*T0*)	H	19.3	4.4	10.38	−298	−15.6	−41.0	0.873
1c ($T0^A$)	H	32.0	13.6	11.83	−301	−15.8	−37.6	0.860
1d ($T0^D$)	H	29.4	12.1	8.60	−246	−17.1	−39.1	0.855
1e ($T0^{4,D}$)	H	30.6	9.8	8.79	−211	−16.1	−35.6	0.820
1f ($T0^{A,D}$)	H	26.6	5.4	7.52	−218	−16.5	−37.2	0.809
				[24]pentaphyrins				
2a (*T0*)	H	11.2	−11.0	−10.95	314	22.3	64.6	0.647
2b (*T1*)	M	24.9	6.2	5.06	−101	−6.7	−14.8	0.725
2c ($T0^A$)	H	19.3	−2.4	−13.47	307	17.0	51.7	0.619
2d ($T1^A$)	M	14.5	1.2	2.60	−66	−9.0	−15.0	0.698
2e ($T0^{A,D}$)	H	11.5	−2.9	−5.28	129	6.6	19.1	0.624
2f ($T0^{4,D}$)	H	15.9	−2.7	−8.16	275	18.6	59.4	0.590

[a] ISE_{corr} and $\Delta\eta$ are given in kcal mol^{-1}, Λ in ppm cgs, and NICS indices in ppm. [b] H and M denote Hückel and Möbius topology, respectively.

dx.doi.org/10.1021/jo4003823 | J. Org. Chem. 2013, 78, 4419−4431

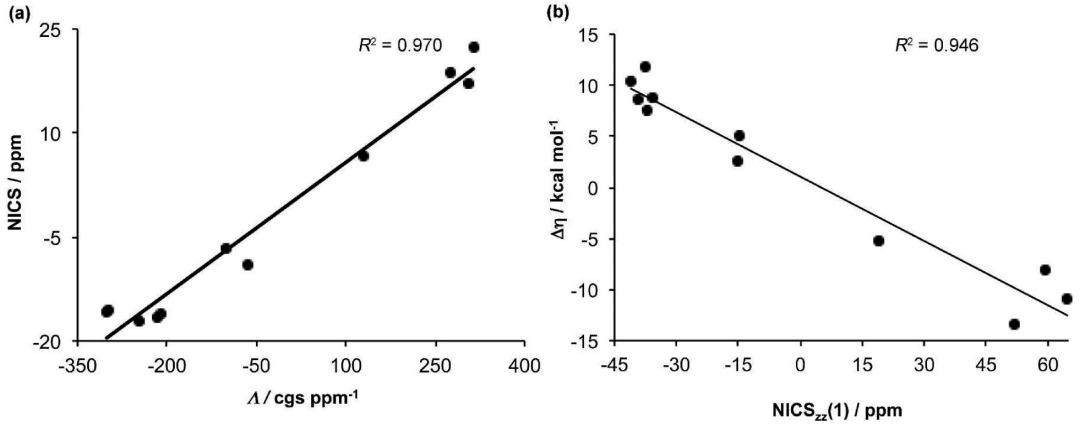

Figure 5. (a) Correlation between the magnetic susceptibility exaltation (Λ) and the isotropic NICS for the studied pentaphyrins. (b) Correlation between the out-of-plane component of the NICS tensor computed at 1 Å [NICS$_{zz}$(1)] and the relative hardness (Δη).

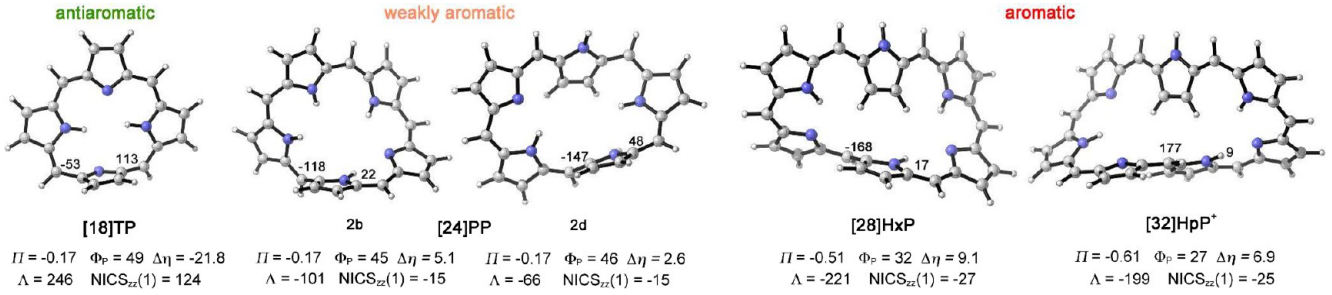

Figure 6. B3LYP/6-31G(d,p)-optimized geometries of Möbius conformers for regular porphyrin, [24]pentaphyrin (**2b** and **2d**), [28]hexaphyrin, and protonated [32]heptaphyrin. Dihedral angles (deg) around the molecular twist, torsional descriptors, and aromaticity indices are shown.

A close relationship between the molecular topology, the number of π-electrons in the CP, and the macrocyclic aromaticity exists. All the Hückel conformations with [22] π-electrons (**1a**–**f**) are strongly aromatic, with positive ISE$_{corr}$ and Δη values, highly negative Λ and NICS values, as well as a bond-delocalized structure. On the contrary, all the Hückel conformations of [24]PP are antiaromatic since they are energetically destabilized and exhibit bond-localized structures and strong paramagnetic ring currents. Consistent with Heilbronner's prediction, the sign of the aromaticity descriptors is reverse for Möbius conformations **2b** and **2d**. The magnetic properties of **2b** and **2d** support weak diatropic ring currents. Therefore, we have demonstrated that the annulene model qualitatively works for the nonfused pentaphyrins(1.1.1.1.1).

All of the predictions were fulfilled by the different aromaticity descriptors except ISE values, which turned out to be positive in all cases. Owing to the unbalanced *s*-cis and *s*-trans diene conformations at both sides of the isomerization reaction, the application of the *syn-anti* corrections on the ISE values is mandatory (Figures S7 and S8, Supporting Information).[52] Accordingly, ISE$_{corr}$ is positive for Hückel **1a**–**f** and Möbius **2b**–**d** conformations and negative for the Hückel topologies with [24] π-electrons. But to what extent are pentaphyrins stabilized/destabilized by aromaticity/antiaromaticity? At the same level of theory, the ISE$_{corr}$ value computed for benzene is 34 kcal mol^{-1}, which corresponds to 5.6 kcal mol^{-1} per carbon. This value is much bigger than the ISE$_{corr}$ values computed for **1a**–**f**.[53] In the case of the Möbius topologies **2b** and **2d**, the aromatic stabilization is even lower (6.2 and 1.2 kcal mol^{-1}) due to the overly dihedrals angle along the CP which prevent effective delocalization. On the other hand, the Hückel conformations with one or two inverted pyrrole rings (**2c**,**e**–**f**) are only destabilized by 2–3 kcal mol^{-1} (−0.13 kcal mol^{-1} per atom). This explains why Hückel antiaromatic [24]pentaphyrins are also viable.

Although aromaticity does not play an important role in stabilizing the Hückel or Möbius conformation in [24]PP, the magnetic properties are greatly influenced by their macrocyclic π-conjugation. The magnetic descriptors reveal strong diatropic ring currents in the aromatic Hückel [22]PP and strong paratropic ones in the antiaromatic Hückel [24]PP. The strength of the induced ring current is related to the efficiency of π-conjugation. Thus, the conformations with small absolute values of Π (**2b** and **2d**) exhibit weaker ring currents.

Excellent correlations (R > 0.985) exist between all the magnetic descriptors (Table S3, Supporting Information). The isomerization method provides exaltation values Λ strongly correlated with the different NICS descriptors (Figure 5a). Also, a very good correlation (R = 0.998) is found between the different NICS-based indices, so the isotropic values computed at the heavy atom center can be used as a reliable descriptor of the aromaticity of pentaphyrins. The main drawback of the magnetic indices (specially Λ) is their dependence on the ring size. Consequently, the exaltation and NICS values of pentaphyrins are higher than that computed for benzene.

Remarkably, the relative hardness (Δη) is very well correlated with the magnetic descriptors (R ranging from 0.973 to 0.992, Figure 5b). In addition, good correlations exist between the structural descriptor HOMA and the reactivity descriptor (R = 0.93). All the diatropic and paratropic pentaphyrins have positive and negative relative hardness, respectively. This conceptual DFT based descriptor[35,54] is easily computed using the

dx.doi.org/10.1021/jo4003823 | J. Org. Chem. 2013, 78, 4419–4431

Scheme 3. Plausible Reaction Mechanism for the Formation of the *N*-Fused Pentaphyrins

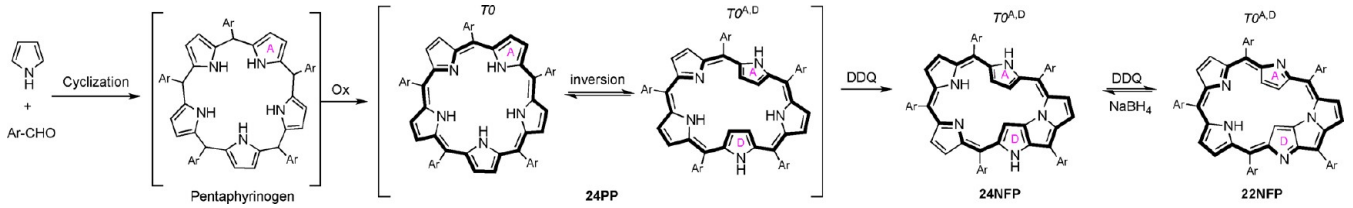

Table 3. Gibbs Free Energies (ΔG_{298}), Enthalpies (ΔH_{298}), Entropies (ΔS_{298}), and Ring Strain Variation ($\Delta\Phi_p$) for the N-Fusion Reaction PP→NFP of the Different Conformations[a]

[22]PP	ΔG_{298}	ΔH_{298}	ΔS_{298}	$\Delta\Phi_p$	[24]PP	ΔG_{298}	ΔH_{298}	ΔS_{298}	$\Delta\Phi_p$
1c ($T0^{A}$)	−16.5	−17.6	−3.8	−17	**2c** ($T0^{A}$)	−21.7	−23.4	−5.6	−17
1d ($T0^{D}$)	−16.7	18.0	−4.3	−17	**2d** ($T1^{A}$)	−25.1	−24.0	3.5	−7
1e ($T0^{4,D}$)	3.9	2.6	−4.2	5	**2e** ($T0^{A,D}$)	−24.9	−27.1	−7.2	−15
1f ($T0^{A,D}$)	−21.5	−23.3	−6.2	−9	**2f** ($T0^{4,D}$)[b]	−20.0	−21.5	−5.0	6

[a] ΔG_{298}, ΔH_{298}, and ΔS_{298} are given in kcal mol^{-1} and $\Delta\Phi_p$ in deg. [b] The N-fusion reaction of **2f** led to a Möbius [24]NFP.

isomerization method without the application of the *syn-anti* corrections. Importantly, this index is not size-dependent, and it can be applied to different-sized compounds.

Figure 6 shows the Möbius conformers computed for several expanded porphyrins together with their torsional descriptors and aromaticity indices. Torsional strain significantly decreases with the size of the macrocycle and the overlap of the π-orbitals is quite effective in the Möbius topologies of [28]hexaphyrin and protonated [32]heptaphyrin, resulting in a distinct macrocyclic aromaticity. On the contrary, the large torsional angles around the molecular twist preclude effective overlap in the Möbius porphyrin and singly twisted pentaphyrins. The Möbius pentaphyrins **2b** and **2d** are slightly aromatic according to a variety of criteria, although less aromatic than larger Möbius expanded porphyrins.

The energetic descriptor ISE_{corr} is weakly correlated with the rest of the aromaticity indices. The magnetic and reactivity-based aromaticity orders do not follow their computed ISE_{corr} orders. Such discrepancies arise from the multifaceted nature of aromaticity, which is specially pronounced for the porphyrinoids.[50] The fact that the ISE_{corr} value computed for the totally planar conformation **1a** is lower than the conformations with one inverted pyrrole ring **1c** and **1d** could indicate that additional effects (such as strain and hyperconjugation[42]) may perturb the isomerization energies. Therefore, we recommend the use of the magnetic and reactivity indices to quantify the aromaticity and antiaromaticity of the pentaphyrins rather than energetic ones.

N-Fusion Reaction in [22]- and [24]Pentaphyrins. Since fully *meso*-arylpentaphyrins(1.1.1.1.1) are always isolated as *N*-fused products, we examined the N-fusion reaction of [22] and [24]PP. Two different reaction mechanisms were proposed for the unexpected formation of NFP.[23a] In the first mechanism, the N-fused products are derived directly from the putative precursor pentaphrynogen during the oxidation process. On the other hand, the second mechanism (Scheme 3) involves the formation of a nonfused [24]pentaphyrin in which two pyrrole rings are inverted, and then oxidized to [24]NFP and/or [22]NFP depending on the amount of DDQ used in the oxidation step.[23b] Interestingly, [22]NFP and [24]NFP forms are easily interconvertible through two-electron redox reactions. If the oxidation proceeds via the second route, nonfused pentaphyrins could be synthetized. The fact that very recently the synthesis of a nonfused [22]pentaphyrin with a free *meso*-position has been reported supports the second mechanism.[27]

The free energies (ΔG_{298}), enthalpies (ΔH_{298}), and entropies (ΔH_{298}) computed for the N-fusion reaction of the different conformers of [22] and [24]pentaphyrins are collected in Table 3. 2,3-Dichloro-5,6-dicyano-1,4-benzoquinone (DDQ) was used as oxidant, being reduced to the corresponding hydroquinone (DDQH2). The N-fusion reactions PP→NFP for both oxidation states are displayed in Figure S11 (Supporting Information). Only the conformations with, at least, one inverted pyrrole ring have been considered since they have the correct geometry for the C−N bond formation.

The C···N distance ranges between 2.80 and 3.05 Å in the singly and doubly inverted nonfused pentaphyrins. On the basis of the very negative ΔG_{298} values, [24]PP are unstable, and they are spontaneously transformed into [24]NFP regardless of the conformation. The release of ring strain is the thermodynamic driving force in the N-fusion reaction, as revealed by $\Delta\Phi_p$. Similar NICS values were computed for the nonfused conformers and their fused counterparts, so aromaticity of the macrocycle hardly changes in the process (Figure S11, Supporting Information). Only, the N-fusion reaction of **2f** involves a topology change from Hückel to Möbius, so a large change in NICS values is observed.

In the case of [22]PP, conformers **1c**, **1d**, and **1f** are prone to undergo an N-fusion reaction which lowers the overall strain in the macrocycle, as seen in $\Delta\Phi_p$. However, **1e** is considerably more stable and is not converted into the N-fused product spontaneously ($\Delta G_{298} > 0$). In **1e**, the N-fusion reaction increases the ring strain. These different behaviors led us to hypothesize that stable nonfused [22]pentaphyrins could be formed if they adopt a $T0^{4,D}$ conformation. Interestingly, the X-ray diffraction analysis revealed a nonfused $T0^{4,D}$ structure for the bis-rhodium(I) complex of the mono-*meso*-free [22]-pentaphyrin.[27]

Dual Descriptor in Nonfused Pentaphyrins. The reactivity of the most important conformers ($T0^{4,D}$ and $T0^{A,D}$) of nonfused pentaphyrins has been analyzed using the dual descriptor $[f^{(2)}(r)]$. In conceptual density functional theory, the dual descriptor is defined as[55]

$$f^{(2)}(r) = \left(\frac{\partial^2\rho(r)}{\partial^2 N}\right)_{\nu(r)} \quad (2)$$

dx.doi.org/10.1021/jo4003823 | J. Org. Chem. 2013, 78, 4419−4431

where N is the total number of electrons, $\rho(r)$ is the electron density, and $\nu(r)$ is the external potential, the framework formed by all atomic nuclei of the system. Within the finite difference approximation:

$$f^{(2)}(r) \approx \rho_{N+1}(r) - 2\rho_N(r) + \rho_{N-1}(r) \quad (3)$$

Here, $\rho_N(r)$, $\rho_{N+1}(r)$, and $\rho_{N-1}(r)$ denote the electron density of the neutral system, anion, and cation, respectively. The dual descriptor is positive in electrophilic regions (that are better at accepting electrons) and negative in nucleophilic regions (that are better at donating electrons). Therefore, a plot of $f^{(2)}(r)$ gives a picture of the "dual" electron-accepting and electro-donating capabilities of a molecule. Favorable chemical reactions occur when regions that are good electron acceptors ($f^{(2)} > 0$) are aligned with regions that are good electron donors ($f^{(2)} < 0$).

The dual descriptor has been established as the key reactivity indicator for pericyclic reactions, where reagents accept and donate electrons concurrently.[56] Very recently, this reactivity descriptor have been successfully applied to predict the active electrophilic center in Ag(III) complex of N-confused porphyrin.[57] Here, the intrinsic reactivity of nonfused [24]PP and [22]PP when interacting with DDQ can be rationalized using the dual descriptor. The dual descriptor isosurfaces of **2e**−**f** and **1e** and DDQ computed at B3LYP/6-31+G(d,p) level of theory is shown in Figure 7.

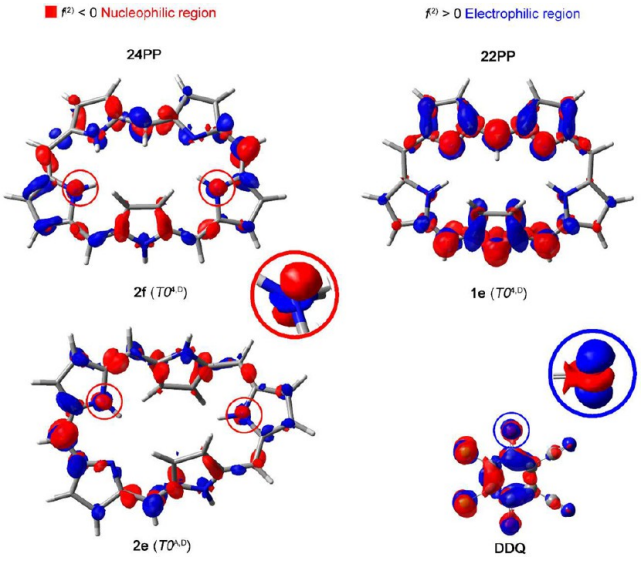

Figure 7. Dual descriptor isosurfaces (0.002 au) for the $TO^{4,D}$ and $TO^{A,D}$ conformers of nonfused pentaphyrins and DDQ.

Different reactivity patterns are found for [24]- and [22]-pentaphyrins. For each conformation, the blue and red regions for $f^{(2)}(r)$ invert after oxidation with DDQ. Interestingly, the reactivity of the pyrrolic nitrogen atoms, involved in the N-fusion reaction, is dependent on the conformation and the oxidation state. In **2f** and **2e**, the pyrrolic nitrogen atoms are nucleophilic centers that interact favorably with the electrophilic carbonyl group of DDQ. However, the pyrrolic nitrogens in the stable nonfused [22]PP **1e** are not reactive, explaining why it can be isolated as a nonfused counterpart.

Conformational Control of Pentaphyrins by *Meso*-Substituents. To determine the optimum conditions for viable nonfused pentaphyrins, the influence of the nature and number of *meso*-substituents on the conformations of [22]PP and [24]PP was investigated. Three substituents (CF_3, C_6F_5, 2,6-Cl_2-phenyl) were considered. The relative energies of the different conformations computed at the B3LYP/6-31G(d,p) level are collected in Table 4.

Conformational preference and chemical stability of nonfused pentaphyrins strongly depends on *meso*-substituents and the oxidation state.[58] The convex conformations are highly destabilized by *meso*-substituents for both oxidation levels. Unlike the planar convex conformation of the unsubstituted [22]PP, a highly distorted *T0* conformation was revealed in the optimized geometries of *meso*-substituted pentaphyrins (Figure S14, Supporting Information). In [24]PP, the optimization of the TO^{A} conformation with five *meso*-substituents led to a triangular structure ($TO^{A,D}$) in all cases.

The triangular conformation with two stacked pyrrole rings is preferred for fully *meso*-aryl-substituted pentaphyrins irrespective of the oxidation state. This conformation is very prone to undergo a N-fusion reaction. The formation of the N-fused structures from this doubly inverted conformation is thermodynamically spontaneous in both [22]PP and [24]PP, as shown in Figure 8. These results explain why fully *meso*-aryl-substituted pentaphyrins exist only as N-fused forms.[23] Among the two reaction pathways shown in Figure 8, the oxidation to [24]NFP is thermodynamically favored, confirming the reaction mechanism shown in Scheme 3. The $TO^{4,D}$ conformation is disfavored owing to the steric repulsion of the inward-facing substituent. The larger steric hindrance of the (2,6)-dichlorophenyl group further destabilizes the $TO^{4,D}$ conformation, which shows a large distortion at the *meso* position 4.

Interestingly, the removal of one *meso*-aryl substituent led to a drastic conformational change in the [22]PP from the triangular to the $TO^{4,D}$ structure, which does not undergo the N-fusion reaction. In that case, the triangular conformation is 13−15 kcal mol^{-1} less stable than the $TO^{4,D}$ conformer. In spite of the tilted pyrrole ring, the $TO^{4,D}$ structure is roughly planar with a mean-plane deviation of 0.302 Å, assuring effective π conjugation over the macrocycle (Π = 0.80). In addition, this conformation is predicted to have a high degree of aromaticity by both magnetic and structural criteria (NICS = −15.5 ppm and HOMA = 0.78).

Remarkably, the intrinsic strain of the nonfused $TO^{4,D}$ structure is strongly dependent on the number of aryl groups. Thus, the torsional strain descriptor Φ_p decreases from 39° to 15° by removing one *meso*-2,6-dichlorophenyl substituent, which enhances the chemical stability of the nonfused pentaphyrins (Table S4). The computed Gibbs free energies point out that [24]PP is oxidized to nonfused [22]PP, in the case of pentaphyrins with a free *meso* position. The isomerization to the N-fused pentaphyrin is not spontaneous since positive free energies are obtained for the interconversion [22]PP→[22]NFP irrespective of the aryl group. In that case, the nonfused $TO^{4,D}$ structure has the lowest torsional strain.

The noncovalent interactions (NCI) in the $TO^{4,D}$ conformation of *meso*-pentafluorophenyl-substituted [22]PP with four (**8**) and five (**7**) aryl groups were conveniently visualized using the recently developed NCI method.[59] This method is capable of distinguishing hydrogen bonds, van der Waals interactions and repulsive steric clashes, based on the peaks that appear in the reduced density gradient (s) at low densities. In this approach, the sign of the second Hessian value (λ_2) is used to distinguish between attractive and repulsive interactions and its strength is derived from the density values of the low-gradient spikes.

The results of the NCI analysis of [22]pentaphyrins **7** and **8** are shown in Figure 9. The severe steric crowding of the inward-

dx.doi.org/10.1021/jo4003823 | J. Org. Chem. 2013, 78, 4419−4431

Table 4. Conformational Relative Energies (in kcal mol^{-1}) of *Meso*-Substituted Nonfused Pentaphyrins

conformer		H	$C_6H_3Cl_2$		C_6F_5		CF_3
Tn^X		**1**	**5**	**6**	**7**	**8**	**9**
[**22**]**PP**	no.[a]	5	5	4	5	4	5
T0 (H)		0.00	4.53	10.56	8.81	18.44	6.48
$T0^A$ (H)		4.86	6.14	21.23	9.93	23.89	13.49
$T0^D$ (H)		7.09	9.06	10.56	11.67	15.94	14.08
$T0^{4,D}$ (H)		0.09	8.53	0.00	1.43	0.00	0.00
$T0^{A,D}$ (H)		15.15	0.00	14.55	0.00	13.03	12.01
[**24**]**PP**							
T0 (H)		0.00	6.54	4.57	7.47	4.27	9.23
T1 (M)		2.80	6.17	7.78	5.30	9.82	*T0*
$T1^A$ (M)		5.06	$T0^{A,D}$	$T0^{A,D}$	$T0^{A,D}$	$T0^{A,D}$	0.00
$T0^{A,D}$ (H)[b]		4.76	0.00	0.00	0.00	0.00	0.32
$T0^{A,D}$ (H)[c]		4.69	2.65	4.41	1.54	5.08	1.70
$T0^{4,D}$ (H)		3.27	$T0^{A,D}$	1.19	7.97	1.29	7.06

[a]No. corresponds to the number of substituents at the *meso* positions. [b]$T0^{A,D}$ corresponds to the triangular conformation with two stacked pyrrole rings. [c]$T0^{A,D}$ corresponds to the triangular conformation with A and D facing toward the same direction.

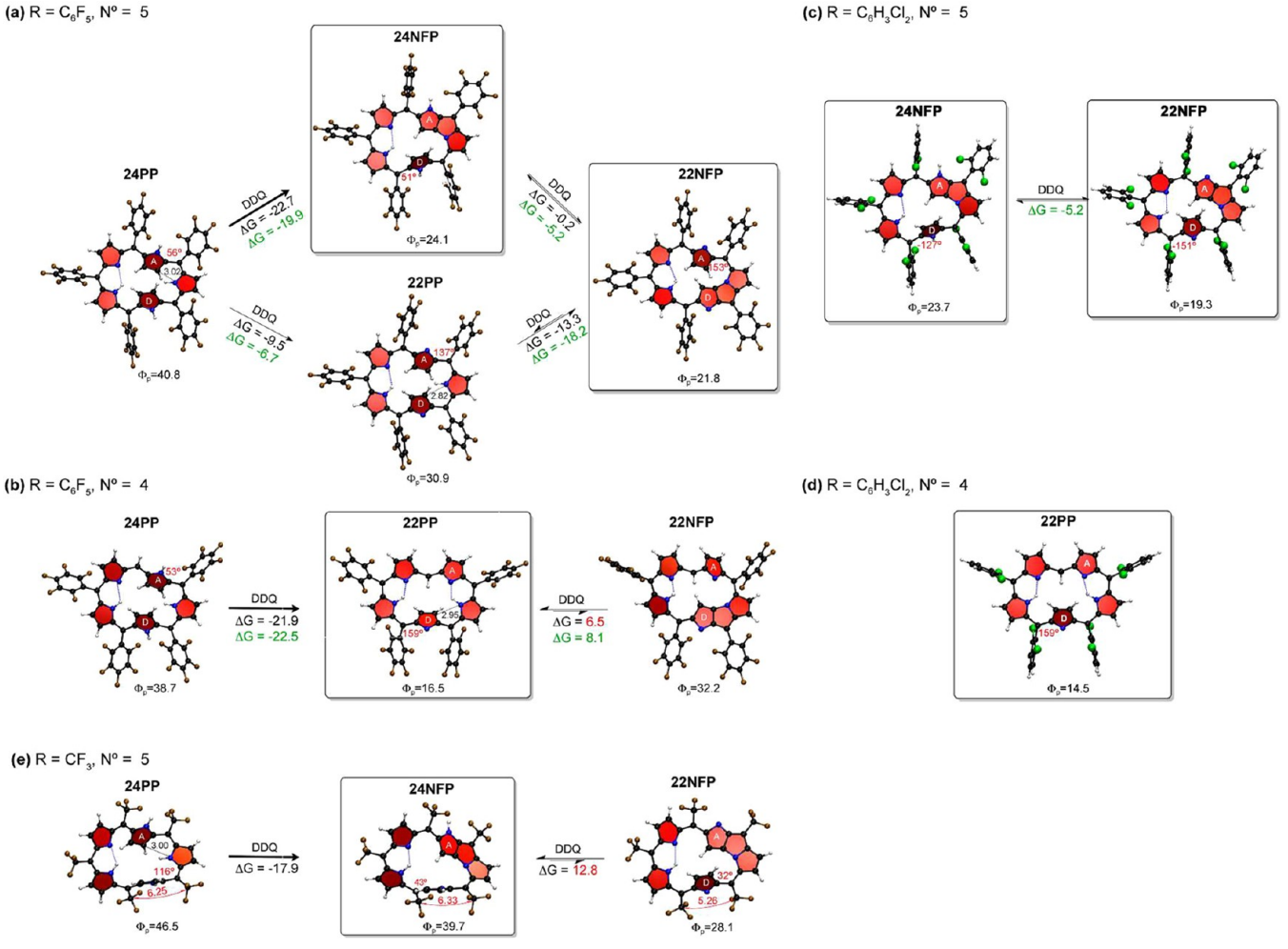

Figure 8. Computed Gibbs free energies (kcal mol^{-1}) for the oxidation/N-fusion reactions of *meso*-substituted pentaphyrins(1.1.1.1.1). The stable forms in each case are highlighted. For the fully *meso*-aryl-substituted pentaphyrins, two different oxidation pathways from the precursor [24]PP are considered: [24]PP→[24]NFP and [24]PP→[22]PP reactions. In (a) and (b) the free energies computed for the *meso*-(2,6)-dichlorophenyl-substituted pentaphyrins are shown in green. The ring strain (Φ_p), the most distorted dihedral angle from planarity along the conjugation pathway, and the C···N distances are also indicated.

pointing pentafluorophenyl group in the $T0^{4,D}$ conformation is dissipated when it is replaced by a hydrogen atom, which is also involved in an attractive CH···π hydrogen bond. The strongest stabilizing interactions correspond to the intramolecular hydrogen bonds in both compounds. The strengthening of the hydrogen bonds when going from **7** to **8** is conveniently

dx.doi.org/10.1021/jo4003823 | J. Org. Chem. 2013, 78, 4419−4431

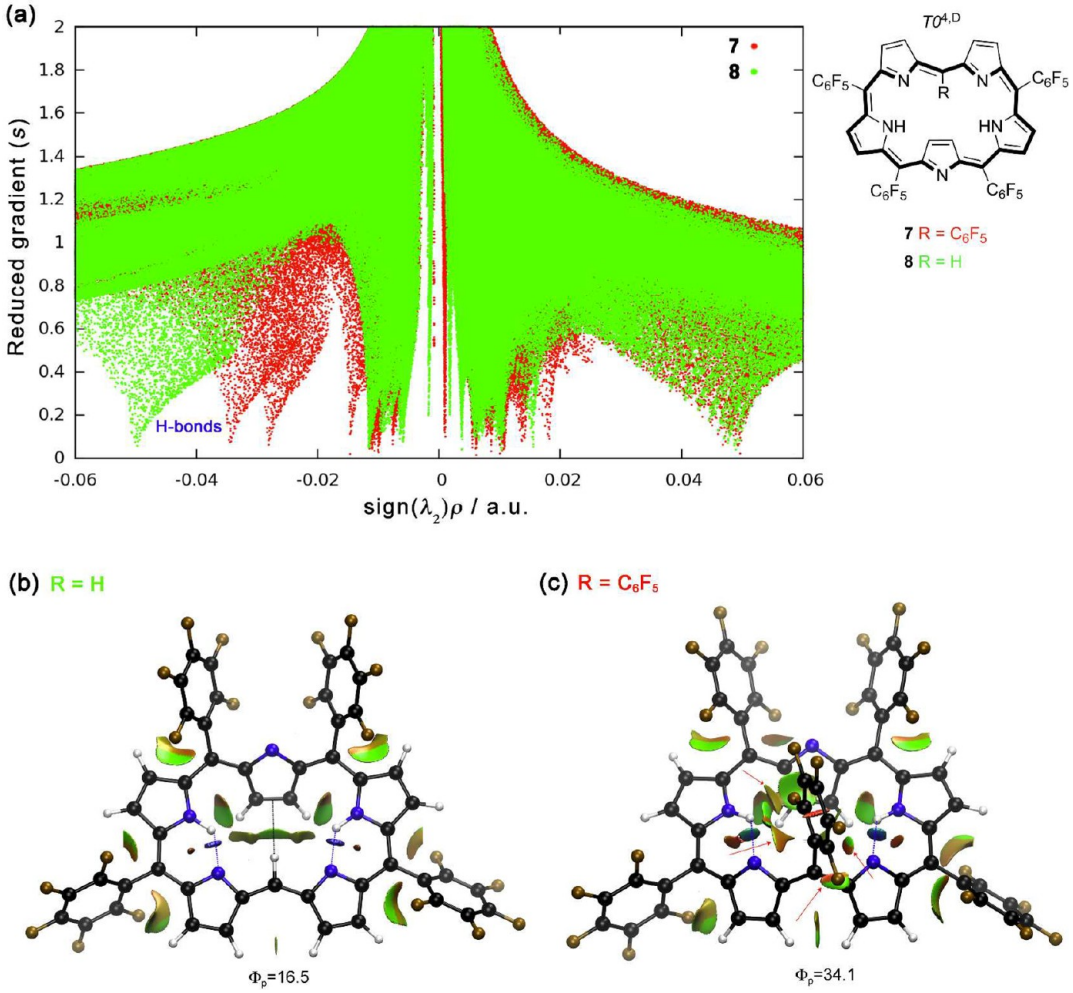

Figure 9. NCI analysis of the $T0^{4,D}$ conformation of *meso*-pentafluorophenyl-substituted [22]PP with five (**7**) and four aryl groups (**8**). (a) Plots of the reduced density gradient (s) vs the electron density multiplied by the sign of the second Hessian eigenvalue. Gradient isosurfaces (s = 0.5 au) of **8** (b) and **7** (c), colored according to values of sign(λ_2)ρ over the range −0.04 to +0.02 au.

visualized with the shift of the characteristic peaks toward bigger density values. The hydrogen-bonding isosurfaces appear at −0.05 au in **8** and at −0.03 in **7**. In addition, there are a number of weakly attractive C−F···X (X = N, H) interactions involving the C_6F_5 groups. Conversely, the isosurfaces around the inward-pointing C_6F_5 group in **7** are mainly repulsive.

The *meso*-trifluoromethyl substituent behaves differently from the aryl groups. The precursor [24]PP prefers a Möbius conformation $T1^A$, which is readily transformed into the [24]NFP in presence of DDQ. The Möbius topology is conserved in the N-fused form, although the macrocyclic conjugation may be rather ineffective (Π = −0.25). In contrast to the reversible redox interconversion between [24]- and [22]NFP bearing *meso*-aryl groups, the oxidation to its [22]NFP counterpart is not allowed with the CF_3 group (Figure 7e) despite the release of strain. In good agreement with the theoretical results, *meso*-(trifluoromethyl)-substituted pentaphyrin was isolated as a [24]NFP with a Möbius solid-state structure, and its oxidation with DDQ/MnO_2 did not yield the corresponding [22]NFP.[60]

The instability of the Hückel [22]NFP seems to be related with the steric hindrance between the bulky CF_3 groups. Whereas in the Möbius [24]NFP the *meso*-substituents adjacent to the tilted pyrrole ring D are in *trans*, separated by 6.33 Å; in the Hückel [22]NFP they are in *cis* with a relative distance of 5.26 Å (Figure 8e). Although the most stable conformation of the nonfused [22]PP corresponds to the $T0^{4,D}$ structure, the computed ΔG for the [24]PP→[22]PP oxidation is −0.7 kcal mol^{-1}. Again, the short distance between two CF_3 groups (5.30 Å) increases the steric crowding in the $T0^{4,D}$ conformation. Therefore, the steric effect plays a major role in determining the Möbius topology of *meso*-trifluoromethyl pentaphyrins.

In summary, the chemical stability of the nonfused pentaphyrin is critically dependent on the number of *meso*-substituents as shown in Figure 8. Fully *meso*-aryl-substituted pentaphyrins adopt a triangular conformation that is transformed into the N-fused species spontaneously. However, the removal of one aryl group prevents the N-fusion reaction, resulting in a stable nonfused $T0^{4,D}$ conformation with [22] π-electrons, almost planar and strongly aromatic. A weakly aromatic N-fused [24]pentaphyrin with Möbius topology is provided by *meso*-trifluoromethyl substituents. Nonfused [24]PP are unstable regardless of the substituents. Importantly, our computational results support the experimental evidence available for *meso*-pentaphyrins(1.1.1.1.1).[23,27,60]

dx.doi.org/10.1021/jo4003823 | J. Org. Chem. 2013, 78, 4419−4431

CONCLUSIONS

The conformational preferences and chemical stability of nonfused [22]- and [24]pentaphyrins(1.1.1.1.1) have been investigated using density functional theory calculations. The conformation of the pentapyrrolic macrocycle is shown to be strongly dependent on the oxidation state, aromaticity of the π-electron system, and substituents at *meso*-positions.

The most stable conformations of the unsubstituted [22]PP correspond to a *T0* and $T0^{4,D}$ structures, almost planar and highly aromatic. The inversion of a pyrrole ring occurs via Möbius transition structures and requires relatively high activation energy barriers (E_a =27 kcal mol^{-1}). Conversely, [24]PP exhibits higher conformational flexibility and Hückel antiaromatic and Möbius conformers coexist in dynamic equilibrium (E_a = 1−7 kcal mol^{-1}). It is shown that the conformational stabilities of [22]conformers are mainly governed by torsional strain.

A close relationship between the molecular topology, the number of π-electrons in the CP, and aromaticity is revealed by energetic, magnetic, reactivity, and structural criteria. Hückel conformations with [22] π-electrons exhibit strong diamagnetic ring currents, whereas strong paramagnetic ones are exhibited by Hückel [24]PP. The Möbius [24]pentaphyrins do not exhibit a distinct macrocyclic aromaticity. The large dihedral angles preclude effective delocalization. According to the correlation analysis, the best indices to quantify the aromaticity of pentaphyrins are the magnetic descriptors (NICS, Λ) and the relative hardness ($\Delta\eta$).

The N-fusion reaction is thermodynamically favored in [24]pentaphyrins due to the release of ring strain, regardless of the conformation. On the contrary, the $T0^{4,D}$ conformer is not transformed into the N-fused form in the [22]PP. Therefore, we hypothesize that stable nonfused [22]pentaphyrins could be isolated if the macrocycle adopts a $T0^{4,D}$ conformation.

Importantly, conformational control of pentaphyrins can be achieved by changing the number of *meso*-substituents. With five aryl groups, [24]PP adopts a triangular conformation $T0^{A,D}$ with two-inverted pyrrole rings that is oxidized to the N-fused counterpart supporting the proposed reaction mechanism. Interestingly, a large structural change in [22]PP is caused by the removal of one aryl group, resulting in a stable nonfused $T0^{4,D}$ conformation. A Möbius topology is preferred by CF_3 substituents, which undergoes a facile N-fusion reaction to give a Möbius N-fused pentaphyrin with [24] π-electrons. It is shown that the conformational relative energies and thermochemistry computed with B3LYP are in excellent agreement with all the experimental data available for *meso*-substituted pentaphyrins(1.1.1.1.1).

ASSOCIATED CONTENT

Supporting Information

Conformational descriptor and nomenclature, interrelation between the ring strain parameters, conformational interconversion pathways in nonfused [22]- and [24]PP, B3LYP-D relative energies, solvation effects, dependence between the relative energies and hydrogen-bonding, ring strain and aromaticity, *syn-anti* corrections for the isomerization stabilization energies, relationships between aromaticity indices, dual descriptor in nonfused pentaphyrins, conformations, and relative energies of *meso*-substituted pentaphyrins and optimized geometries. This material is available free of charge via the Internet at http://pubs.acs.org.

AUTHOR INFORMATION

Corresponding Author

*E-mail: malonsog@vub.ac.be.

Notes

The authors declare no competing financial interest.

ACKNOWLEDGMENTS

M.A. thanks the European Community for financial support through the postdoctoral fellowship FP7-PEOPLE-2010-IEF-273527. P.G. and F.D.P thank the Fund for Scientific Research−Flanders (FWO) and the Free University of Brussels (VUB) for continuous support of their group.

REFERENCES

(1) Heilbronner, E. *Tetrahedron Lett.* **1964**, *5*, 1923.
(2) Ajami, D.; Oeckler, O.; Simon, A.; Herges, R. *Nature* **2003**, *426*, 819.
(3) (a) Castro, C.; Chen, Z.; Wannere, C. S.; Jiao, H.; Karney, W. L.; Mauksch, M.; Puchta, R.; Hommes, N. J. R. v. E.; Schleyer, P. v. R. *J. Am. Chem. Soc.* **2005**, *127*, 2425. (b) Ajami, D.; Hess, K.; Köhler, F.; Näther, C.; Oeckler, O.; Simon, A.; Yamamoto, C.; Okamoto, Y.; Herges, R. *Chem.—Eur. J.* **2006**, *12*, 5434.
(4) (a) Castro, C.; Karney, W. L.; Valencia, M. A.; Vu, C. M. H.; Pemberton, R. P. *J. Am. Chem. Soc.* **2005**, *127*, 9704. (b) Pemberton, R. P.; McShane, C. M.; Castro, C.; Karney, W. L. *J. Am. Chem. Soc.* **2006**, *128*, 16692. (c) Spitler, E. L.; Johnson, C. A.; Haley, M. M. *Chem. Rev.* **2006**, *106*, 5344. (d) Mohebbi, A. R.; Mucke, E.-K.; Schaller, G. R.; Köhler, F.; Sönnichsen, F. D.; Ernst, L.; Näther, C.; Herges, R. *Chem.—Eur. J.* **2010**, *16*, 7767.
(5) For excellent recent reviews, see: (a) Saito, S.; Osuka, A. *Angew. Chem., Int. Ed.* **2011**, *50*, 4342. (b) Stępień, M.; Sprutta, N.; Latos-Grażyński, L. *Angew. Chem., Int. Ed.* **2011**, *50*, 4288.
(6) (a) Misra, R.; Chandrashekar, T. K. *Acc. Chem. Res.* **2008**, *41*, 265. (b) Yoon, Z. S.; Osuka, A.; Kim, D. *Nature. Chem.* **2009**, *1*, 113. (c) Roznyatovskiy, V. V.; Lee, C.-H.; Sessler, J. L. *Chem. Soc. Rev.* **2013**, *42*, 1921.
(7) Stępień, M.; Latos-Grażyński, L.; Sprutta, N.; Chwalisz, P.; Szterenberg, L. *Angew. Chem., Int. Ed.* **2007**, *46*, 7869.
(8) (a) Sankar, J.; Mori, S.; Saito, S.; Rath, H.; Suzuki, M.; Inokuma, Y.; Shinokubo, H.; Suk Kim, K.; Yoon, Z. S.; Shin, J.-Y.; Lim, J. M.; Matsuzaki, Y.; Matsushita, O.; Muranaka, A.; Kobayashi, N.; Kim, D.; Osuka, A. *J. Am. Chem. Soc.* **2008**, *130*, 13568. (b) Higashino, T.; Inoue, M.; Osuka, A. *J. Org. Chem.* **2010**, *75*, 7958.
(9) (a) Saito, S.; Shin, J. Y.; Lim, J. M.; Kim, K. S.; Kim, D.; Osuka, A. *Angew. Chem., Int. Ed.* **2008**, *47*, 9657. (b) Yoon, M. C.; Shin, J. Y.; Lim, J. M.; Saito, S.; Yoneda, T.; Osuka, A.; Kim, D. *Chem.—Eur. J.* **2011**, *17*, 6707.
(10) Lim, J. M.; Shin, J.-Y.; Tanaka, Y.; Saito, S.; Osuka, A.; Kim, D. *J. Am. Chem. Soc.* **2010**, *132*, 3105.
(11) Tanaka, Y.; Saito, S.; Mori, S.; Aratani, N.; Shinokubo, H.; Shibata, N.; Higuchi, Y.; Yoon, Z. S.; Kim, K. S.; Noh, S. B.; Park, J. K.; Kim, D.; Osuka, A. *Angew. Chem., Int. Ed.* **2008**, *47*, 681.
(12) (a) Shin, J.-Y.; Lim, J. M.; Yoon, Z. S.; Kim, K. S.; Yoon, M.-C.; Hiroto, S.; Shinokubo, H.; Shimizu, S.; Osuka, A.; Kim, D. *J. Phys. Chem. B* **2009**, *113*, 5794. (b) Koide, T.; Youfu, K.; Saito, S.; Osuka, A. *Chem. Commun.* **2009**, 6047.
(13) (a) Tokuji, S.; Shin, J.-Y.; Kim, K. S.; Lim, J. M.; Youfu, K.; Saito, S.; Kim, D.; Osuka, A. *J. Am. Chem. Soc.* **2009**, *131*, 7240. (b) Inoue, M.; Kim, K. S.; Suzuki, M.; Lim, J. M.; Shin, J.-Y.; Kim, D.; Osuka, A. *Angew. Chem., Int. Ed.* **2009**, *48*, 6687. (c) Lim, J. M.; Inoue, M.; Sung, Y. M.; Suzuki, M.; Higashino, T.; Osuka, A.; Kim, D. *Chem. Commun.* **2011**, *47*, 3960.
(14) (a) Stępień, M.; Szyszko, B.; Latos-Grazynski, L. *J. Am. Chem. Soc.* **2010**, *132*, 3140. (b) Yoon, M. C.; Kim, P.; Yoo, H.; Shimizu, S.; Koide, T.; Tokuji, S.; Saito, S.; Osuka, A.; Kim, D. *J. Phys. Chem. B* **2011**, *115*, 14928. (c) Torrent-Sucarrat, M.; Anglada, J. M.; Luis, J. M. *J. Chem. Phys.* **2012**, *137*, 184306. (d) Kim, K. S.; Yoon, Z. S.; Ricks, A. B.; Shin, J.-Y.;

Mori, S.; Sankar, J.; Saito, S.; Jung, Y. M.; Wasielewski, M. R.; Osuka, A.; Kim, D. *J. Phys. Chem. A* **2009**, *113*, 4498.
(15) (a) Jux, N. *Angew. Chem., Int. Ed.* **2008**, *47*, 2543. (b) Osuka, A.; Saito, S. *Chem. Commun.* **2011**, *47*, 4330.
(16) Shin, J. Y.; Kim, K. S.; Yoon, M. C.; Lim, J. M.; Yoon, Z. S.; Osuka, A.; Kim, D. *Chem. Soc. Rev.* **2010**, *39*, 2751.
(17) Lim, J. M.; Yoon, Z. S.; Shin, J.-Y.; Kim, K. S.; Yoon, M.-C.; Kim, D. *Chem. Commun.* **2009**, 261.
(18) (a) Senge, M. O.; Fazekas, M.; Notaras, E. G. A.; Blau, W. J.; Zawadzka, M.; Locos, O. B.; Mhuircheartaigh, E. M. N. *Adv. Mater.* **2007**, *19*, 2737. (b) Pawlicki, M.; Collins, H. A.; Denning, R. G.; Anderson, H. L. *Angew. Chem., Int. Ed.* **2009**, *48*, 3244.
(19) (a) Ikawa, Y.; Takeda, M.; Suzuki, M.; Osuka, A.; Furuta, H. *Chem. Commun.* **2010**, *46*, 5689. (b) Osuka, A.; Tanaka, T.; Mori, H. *J. Mater. Chem. C* **2013**, DOI: 10.1039/C3TC00932G.
(20) Comuzzi, C.; Cogoi, S.; Overhand, M.; Van der Marel, G. A.; Overkleeft, H. S.; Xodo, L. E. *J. Med. Chem.* **2006**, *49*, 196.
(21) Yoon, Z. S.; Cho, D.-G.; Kim, K. S.; Sessler, J. L.; Kim, D. *J. Am. Chem. Soc.* **2008**, *130*, 6930.
(22) Rexhausen, H.; Gossauer, A. *J. Chem. Soc., Chem. Commun.* **1983**, 275.
(23) (a) Shin, J.-Y.; Furuta, H.; Osuka, A. *Angew. Chem., Int. Ed.* **2001**, *40*, 619. (b) Mori, S.; Shin, J.-Y.; Shimizu, S.; Ishikawa, F.; Furuta, H.; Osuka, A. *Chem.—Eur. J.* **2005**, *11*, 2417.
(24) Park, J. K.; Yoon, Z. S.; Yoon, M.-C.; Kim, K. S.; Mori, S.; Shin, J.-Y.; Osuka, A.; Kim, D. *J. Am. Chem. Soc.* **2008**, *130*, 1824.
(25) (a) Bruckner, C.; D. Sternberg, E.; W. Boyle, R.; Dolphin, D. *Chem. Commun.* **1997**, 1689. (b) Comuzzi, C.; Cogoi, S.; Xodo, L. E. *Tetrahedron* **2006**, *62*, 8147. Doubly N-confused oxopentaphyrins were also isolated as stable nonfused macrocycles: (c) Srinivasan, A.; Ishizuka, T.; Maeda, H.; Furuta, H. *Angew. Chem., Int. Ed.* **2004**, *116*, 2951.
(26) Shin, J.-Y.; Furuta, H.; Yoza, K.; Igarashi, S.; Osuka, A. *J. Am. Chem. Soc.* **2001**, *123*, 7190.
(27) Yoneda, T.; Mori, H.; Lee, B. S.; Yoon, M. C.; Kim, D.; Osuka, A. *Chem. Commun.* **2012**, *48*, 6785.
(28) Alonso, M.; Geerlings, P.; De Proft, F. *Chem.—Eur. J.* **2012**, *18*, 10916.
(29) Alonso, M.; Geerlings, P.; De Proft, F. *Chem.—Eur. J.* **2013**, *19*, 1617.
(30) Gaussian 09, Revision B.01: Frisch, M. J.; Trucks, G. W.; Schlegel, H. B.; Scuseria, G. E.; Robb, M. A.; Cheeseman, J. R.; Scalmani, G.; Barone, V.; Mennucci, B.; Petersson, G. A.; Nakatsuji, H.; Caricato, M.; Li, X.; Hratchian, H. P.; Izmaylov, A. F.; Bloino, J.; Zheng, G.; Sonnenberg, J. L.; Hada, M.; Ehara, M.; Toyota, K.; Fukuda, R.; Hasegawa, J.; Ishida, M.; Nakajima, T.; Honda, Y.; Kitao, O.; Nakai, H.; Vreven, T.; Montgomery, J. A., Jr.; Peralta, J. E.; Ogliaro, F.; Bearpark, M.; Heyd, J. J.; Brothers, E.; Kudin, K. N.; Staroverov, V. N.; Kobayashi, R.; Normand, J.; Raghavachari, K.; Rendell, A.; Burant, J. C.; Iyengar, S. S.; Tomasi, J.; Cossi, M.; Rega, N.; Millam, J. M.; Klene, M.; Knox, J. E.; Cross, J. B.; Bakken, V.; Adamo, C.; Jaramillo, J.; Gomperts, R.; Stratmann, R. E.; Yazyev, O.; Austin, A. J.; Cammi, R.; Pomelli, C.; Ochterski, J. W.; Martin, R. L.; Morokuma, K.; Zakrzewski, V. G.; Voth, G. A.; Salvador, P.; Dannenberg, J. J.; Dapprich, S.; Daniels, A. D.; Farkas, Ö.; Foresman, J. B.; Ortiz, J. V.; Cioslowski, J.; Fox, D. J. Gaussian, Inc., Wallingford CT, 2009.
(31) Becke, A. D. *J. Chem. Phys.* **1993**, *98*, 5648.
(32) Grimme, S. *J. Comput. Chem.* **2004**, *25*, 1463.
(33) Schleyer, P. v. R.; Pühlhofer, F. *Org. Lett.* **2002**, *4*, 2873.
(34) Dauben, H. J.; Wilson, J. D.; Layti, J. L. *J. Am. Chem. Soc.* **1968**, *90*, 811.
(35) De Proft, F.; Geerlings, P. *Phys. Chem. Chem. Phys.* **2004**, *6*, 242.
(36) Keith, T. A.; Bader, R. F. W. *Chem. Phys. Lett.* **1993**, *210*, 223.
(37) (a) Schleyer, P. v. R.; Maerker, C.; Dransfeld, A.; Jiao, H. J.; Hommes, N. *J. Am. Chem. Soc.* **1996**, *118*, 6317. (b) Chen, Z.; Wannere, C. S.; Corminboeuf, C.; Puchta, R.; Schleyer, P. v. R. *Chem. Rev.* **2005**, *105*, 3842.
(38) Pearson, R. G. *Chemical Hardness*; Wiley: New York, 1997.
(39) Contreras-García, J.; Johnson, E. R.; Keinan, S.; Chaudret, R.; Piquemal, J.-P.; Beratan, D. N.; Yang, W. *J. Chem. Theory Comput.* **2011**, *7*, 625.
(40) Herges, R. *Chem. Rev.* **2006**, *106*, 4820.
(41) Rappaport, S. M.; Rzepa, H. S. *J. Am. Chem. Soc.* **2008**, *130*, 7613.
(42) Wu, J. I.; Fernández, I.; Mo, Y.; Schleyer, P. v. R. *J. Chem. Theory Comput.* **2012**, *8*, 1280.
(43) Toganoh, M.; Furuta, H. *J. Phys. Chem. A* **2009**, *113*, 13953.
(44) Marcos, E.; Anglada, J. M.; Torrent-Sucarrat, M. *J. Phys. Chem. C* **2012**, *116*, 24358.
(45) Marenich, A. V.; Cramer, C. J.; Truhlar, D. G. *J. Phys. Chem. B* **2009**, *113*, 6378.
(46) Sondheimer, F.; Wolovsky, R.; Amiel, Y. *J. Am. Chem. Soc.* **1962**, *84*, 274.
(47) In both Hückel and Möbius all-pyrrole porphyrinoids, the annulene-like conjugation pathway passes through the iminic nitrogens and circumvents the amino NH groups, as shown in Scheme 1.
(48) (a) Aihara, J.-i. *J. Phys. Chem. A* **2008**, *112*, 5305. (b) Aihara, J.-i.; Makino, M. *J. Mol. Model.* **2009**, *15*, 1427. (c) Aihara, J.-i.; Horibe, H. *Org. Biomol. Chem.* **2009**, *7*, 1939. (d) Aihara, J.-i.; Makino, M. *Org Biomol Chem* **2010**, *8*, 261.
(49) (a) Nakagami, Y.; Sekine, R.; Aihara, J.-i. *Org. Biomol. Chem.* **2012**, *10*, 5219. (b) Aihara, J.-i.; Nakagami, Y.; Sekine, R.; Makino, M. *J. Phys. Chem. A* **2012**, *116*, 11718.
(50) Wu, J. I.; Fernández, I.; Schleyer, P. v. R. *J. Am. Chem. Soc.* **2012**, *135*, 315.
(51) (a) Kruszewski, J.; Krygowski, T. M. *Tetrahedron Lett.* **1972**, *13*, 3839. (b) Krygowski, T. M. *J. Chem. Inf. Comput. Sci.* **1993**, *33*, 70.
(52) Wannere, C. S.; Moran, D.; Allinger, N. L.; Hess, B. A., Jr.; Schaad, L. J.; Schleyer, P. v. R. *Org. Lett.* **2003**, *5*, 2983.
(53) The ISE method evaluates only the aromatic stabilization of nonfused pentaphyrins arising from the annulenic macrocycle but neglects the local aromatic stabilization due to the pyrrole rings. While the magnetic and spectroscopic properties of porphyrinoids arise from their macrocyclic π conjugation, the number of pyrrole rings is more important for determining the thermochemical stability (ref 50).
(54) (a) De Proft, F.; Geerlings, P. *Chem. Rev.* **2001**, *101*, 1451. (b) Geerlings, P.; De Proft, F.; Langenaeker, W. *Chem. Rev.* **2003**, *103*, 1793.
(55) (a) Morell, C.; Grand, A.; Toro-Labbé, A. *J. Phys. Chem. A* **2005**, *109*, 205. (b) Morell, C.; Grand, A.; Toro-Labbé, A. *Chem. Phys. Lett.* **2006**, *425*, 342.
(56) (a) Ayers, P. W.; Morell, C.; De Proft, F.; Geerlings, P. *Chem.—Eur. J.* **2007**, *13*, 8240. (b) Geerlings, P.; Ayers, P. W.; Toro-Labbé, A.; Chattaraj, P. K.; De Proft, F. *Acc. Chem. Res.* **2012**, *45*, 683.
(57) Jiang, H.-W.; Hao, F.; Chen, Q.-Y.; Xiao, J.-C.; Liu, S.-B.; Gu, Y.-C. *J. Org. Chem.* **2010**, *75*, 3511.
(58) A *meso*-substituent in a dipyrrin derivative was found to control the product distribution of the DMSO/$POCl_3$ reaction: Juna, T.; Kim, K.; Lee, K. M.; Murale, D. P.; Singh, A. P.; Natsagdorj, A.; Liew, H.; Suh, Y.-H.; Churchill, D. G. *J. Porphyrins Phthalocyanines* **2012**, *16*, 1201.
(59) (a) Johnson, E. R.; Keinan, S.; Mori-Sánchez, P.; Contreras-García, J.; Cohen, A. J.; Yang, W. *J. Am. Chem. Soc.* **2010**, *132*, 6498. (b) Contreras-Garcia, J.; Yang, W.; Johnson, E. R. *J. Phys. Chem. A* **2011**, *115*, 12983.
(60) Shimizu, S.; Aratani, N.; Osuka, A. *Chem.—Eur. J.* **2006**, *12*, 4909.